

# LOD-GS: Level-of-Detail-Sensitive 3D Gaussian Splatting for Detail Conserved Anti-Aliasing

Zhenya Yang<sup>1</sup> Bingchen Gong<sup>2</sup> Kai Chen<sup>1</sup>

<sup>1</sup> The Chinese University of Hong Kong <sup>2</sup> Ecole Polytechnique

## Abstract

Despite the advancements in quality and efficiency achieved by 3D Gaussian Splatting (3DGS) in 3D scene rendering, aliasing artifacts remain a persistent challenge. Existing approaches primarily rely on low-pass filtering to mitigate aliasing. However, these methods are not sensitive to the sampling rate, often resulting in under-filtering and over-smoothing renderings. To address this limitation, we propose **LOD-GS**, a Level-of-Detail-sensitive filtering framework for Gaussian Splatting, which dynamically predicts the optimal filtering strength for each 3D Gaussian primitive. Specifically, we introduce a set of basis functions to each Gaussian, which take the sampling rate as input to model appearance variations, enabling sampling-rate-sensitive filtering. These basis function parameters are jointly optimized with the 3D Gaussian in an end-to-end manner. The sampling rate is influenced by both focal length and camera distance. However, existing methods and datasets rely solely on down-sampling to simulate focal length changes for anti-aliasing evaluation, overlooking the impact of camera distance. To enable a more comprehensive assessment, we introduce a new synthetic dataset featuring objects rendered at varying camera distances. Extensive experiments on both public datasets and our newly collected dataset demonstrate that our method achieves SOTA rendering quality while effectively eliminating aliasing. The code and dataset are available at <https://github.com/Huster-YZY/LOD-GS>.

## 1. Introduction

Novel view synthesis (NVS) plays a crucial role in the fields of computer vision and computer graphics. Advanced NVS techniques significantly enhance applications in virtual reality, digital modeling, and embodied AI. A notable milestone in NVS is the Neural Radiance Field (NeRF) [27], which represents a 3D scene using a multi-layer perceptron (MLP) and optimizes this MLP through volume ray marching [5, 17, 26] and gradient descent based on multi-view inputs. In comparison to NeRF [27], recent advancements

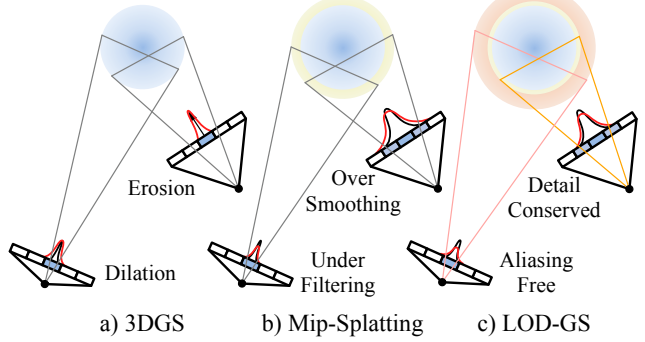


Figure 1. (a) 3DGS treats a 3D Gaussian primitive (in blue) uniformly across different views and applies a dilation operator (in red) before rendering. (b) Mip-Splatting applies the fixed 3D smoothing filter (in yellow) to the primitive across all views. (c) LOD-GS applies different filters (in yellow and orange) based on the sampling rates of the views. Both Mip-Splatting and our LOD-GS utilize an EWA filter (in red) before rendering. The lack of filtering and the use of a dilation operator in 3DGS result in erosion and dilation effects. The fixed 3D smoothing filter in Mip-Splatting leads to over-smoothing and under-filtering.

in 3D Gaussian Splatting (3DGS) [14] offer an alternative approach by representing a 3D scene with a collection of 3D Gaussians. This method benefits from an efficiently implemented CUDA rasterizer, which facilitates real-time rendering and efficient training processes. These advantages position 3DGS as a competitive alternative to NeRF.

However, 3DGS also faces aliasing problems [7] like NeRF. 3DGS is able to achieve good novel view synthesis performance when the training and testing views share roughly the same sampling rate to the observed scene, defined as the ratio of focal length to camera distance. So the aliasing problem of 3DGS is unobvious because existing datasets usually capture a scene from nearly the same distance with the same focal length. For 3DGS models trained on these single-scale datasets, they tend to generate degraded results or aliased renderings when test views zoom in or out significantly. The main reason for this problem is that the 3DGS model is fixed after training. It does not

adjust its appearance according to the sampling rate. This limitation leads to the aliasing and degraded results.

In this paper, we are inspired by the Mipmap technique [41], which is used in computer graphics rendering pipelines to tackle the aliasing. Mipmap involves a collection of progressively downsampled textures, enabling the program to choose the appropriate resolution based on the camera's sampling rate—a technique known as pre-filtering. This method is grounded in the Nyquist-Shannon Sampling Theorem [29, 34] and its concept can be generalized as Level of Detail (LOD) [8, 15, 24, 40], which indicates that the appearance of an object changes with the sampling rate for the scene.

We adopt the Mipmap technique into the 3D Gaussian Splatting framework [14] to represent the pre-filtered radiance field with different levels of detail using multiscale images as input. Because the vanilla 3DGS is not sensitive to the sampling rate, training it with multi-scale images can lead to ambiguity in optimization, making rendering results blur and lack of detail. In this paper, we propose a level-of-detail-sensitive 3DGS framework, named LOD-GS, to effectively sense the change in sampling rate and train the pre-filtered radiance field from pre-filtered images. We propose to add a set of basis functions on each Gaussian primitive to learn the appearance change across different sampling rates. These basis functions take the sampling rate as input and predict the filter size and appearance change for each primitive as illustrated in Figure 1 and Figure 3. The filtered primitive will be splatted into 2D screen space and perform the Elliptical Weighted Average (EWA) filtering [55] to further improve anti-aliasing ability of our method. Besides the framework, we re-render the synthetic dataset used in NeRF [27] from three different camera distances to simulate the changes in sampling rate caused by varying camera distances. The evaluation is carried out on both public datasets [2, 3, 27] and our newly collected dataset. Experiment results demonstrate that our method can disentangle training views with different sampling rates and learn a pre-filtered radiance field from these views, achieving detail-conserved and aliasing-free rendering at the same time.

Our contributions are as follows:

- We introduce **LOD-GS**, a Level-of-Detail-sensitive Gaussian Splatting framework that enables effective anti-aliasing while preserving fine details in rendering results.
- Our proposed LOD-GS eliminates the ambiguity in training caused by inputs with different sampling rates, allowing it to effectively learn a pre-filtered radiance field from pre-filtered images.
- We extend the original NeRF Synthetic Dataset [27] by incorporating rendering views from different camera distances, providing a more comprehensive evaluation of zoom-in and zoom-out effects in neural radiance fields.

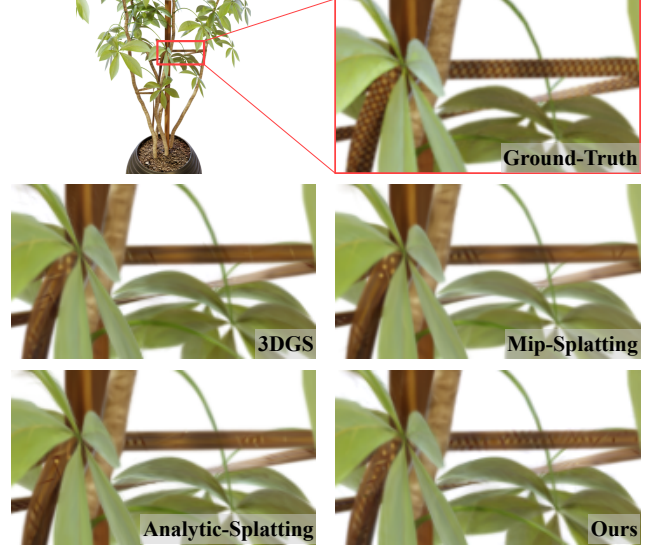


Figure 2. **Comparison of Detail Reconstruction.** All methods are trained on inputs with varying sampling rates. In comparing the reconstruction results of different methods, only our LOD-GS successfully reconstructs the intricate texture of the silk ribbon. Other methods share the smoothing problem to different extents.

## 2. Related Work

**Novel View Synthesis** Novel View Synthesis (NVS) is a fundamental vision task aimed at generating plausible renderings from new camera positions based on a set of input images and their corresponding camera positions. The introduction of Neural Radiance Fields (NeRF) [27] has significantly changed the approach to solving the NVS task. NeRF formulates Novel View Synthesis as a volume rendering and optimization problem. Nearly all subsequent works adhere to this framework. However, due to the frequent querying of the MLP during training and inference, vanilla NeRF [27] is quite slow, requiring over ten hours for training per scene and dozens of seconds to render a new view. Following works have replaced the full implicit representation of NeRF with feature grid-based representations to accelerate training and inference speeds [6, 10, 23, 28, 35]. Some approaches also explore the point-based neural representations [16, 32, 36, 44, 49, 53]. The emergence of 3D Gaussian Splatting [14], which represents the scene as a collection of 3D Gaussians, has removed the MLP from the radiance field representation. This specially designed MLP-free framework, combined with efficient implementation, allows 3DGS to achieve real-time rendering speeds and perform efficient training. Due to these advantages, 3DGS is beginning to replace NeRF in many applications. Vanilla 3DGS is struggle to tackle the aliasing, this paper focuses on enhancing the anti-aliasing capability of 3DGS to achieve aliasing-free and detail conserved rendering.

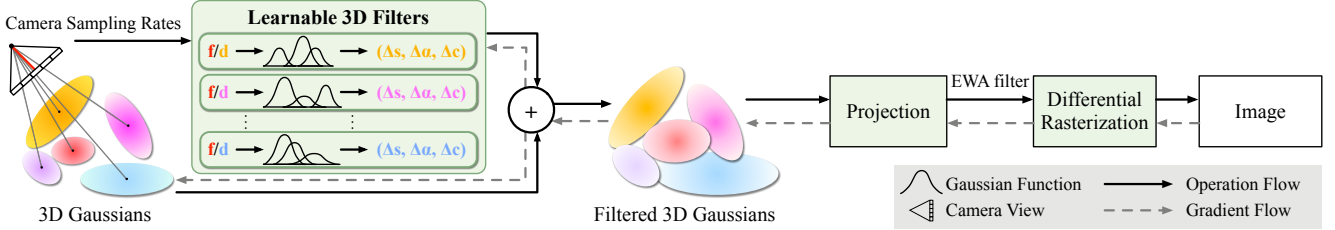


Figure 3. **Overview of our pipeline.** During rendering, the sampling rate for each Gaussian primitive is sent to a learnable module that predicts the appropriate 3D filters for them. The filtered 3D Gaussians are then projected into 2D space and further processed using EWA filter before rasterization. The learnable 3D filters and the 3D Gaussians are jointly optimized end-to-end with image supervision.

**Anti-Aliasing of Neural Radiance Field** Neural rendering methods integrate pre-filtering techniques to mitigate aliasing [2–4, 12, 50, 54]. Mip-NeRF [2] is the first work to address the aliasing problem in NeRF by proposing Integrated Positional Encoding (IPE), which filters out high-frequency components when the camera’s sampling rate is low. Following works [3, 12] speed up the training of Mip-NeRF and extend it to handle unbounded scenes. Due to the differences in rendering methods between NeRF and 3DGS, the anti-aliasing strategy used in NeRF cannot be directly applied to 3DGS. Several methods have recently been proposed to address the aliasing problem in Gaussian Splatting [18, 21, 45, 50]. Multiscale-3DGS (MSGs) [45] represents a 3D scene as a collection of 3D Gaussians of varying levels, selecting only a subset of these levels for rendering based on the target resolution to overcome aliasing. Mip-Splatting [50] introduces the 3D smoothing filter and the 2D mip-filter to remove high-frequency components from the Gaussians. Mipmap-GS [18] utilizes a two stage training and generated pseudo ground truth to adapt to a specific resolution. Analytic-Splatting [21] proposes an approximate method to compute the integration of Gaussian, effectively tackling the aliasing problem. However, all these methods have their limitations. The explicit level representation in MSGs complicates the training and increase the number of primitives. The 3D filter in Mip-Splatting remains fixed after training regardless of the sampling rate of camera, leading to issues of under-filtering and over-smoothing as illustrated in Figure 2. Mipmap-GS needs re-training once the sampling rate changes. For Analytic-Splatting, the introduction of integration slows down its training and rendering. In this paper, we propose a level-of-detail-sensitive filtering strategy to effectively achieve aliasing-free rendering.

#### Additional Parameter Control for Gaussian Primitive

We aim to adjust the degree of filtering applied on Gaussians according to the value of sampling rate. Therefore, we review how existing methods modify the parameters of 3DGS using an additional input variable in this section. Aside from storing the parameter changes at all time steps [25], the remaining approaches can be broadly classi-

fied into three categories. The methods in the first category use MLPs to model parameter changes [13, 42, 47], which has been explored in NeRF area [11, 20, 30, 31, 33, 37, 43, 51]. For instance, 4DGaussians [42] queries a learnable spatial-temporal feature grid using Gaussian positions, then inputs this feature into a neural network to predict spatial shifts and deformations of the primitive. Another category represents a scene as a collection of high-dimensional Gaussians. The additional input is treated as a new dimension of the Gaussian. During rendering, given the value of the input variable on this new axis, the conditioned 3D Gaussians are computed before rendering [9, 48]. The main drawback of this design is that it can easily generate large amounts of high-dimensional Gaussians, leading to overfitting and increased model size. In addition to the above two categories, a different approach to modeling parameter changes is to add a set of learnable basis functions to each Gaussian primitive to capture variations over the input variable [22, 46]. In this paper, we model the filter change of 3DGS using a set of basis functions that take the camera’s sampling rate as input. This design helps us predict the most appropriate filter for aliasing-free rendering in an efficient manner.

## 3. Preliminaries

### 3.1. 3D Gaussian Splatting

Kerbl et al. [14] utilize learnable 3D Gaussian primitives to represent 3D scenes and render different views using a differentiable volume splatting rasterizer. In 3DGS, each 3D Gaussian primitive is parameterized using a 3D covariance matrix  $\Sigma$  and a distribution center  $\mathbf{p}_k$ :

$$\mathcal{G}(\mathbf{p}) = \exp \left( -\frac{1}{2}(\mathbf{p} - \mathbf{p}_k)^\top \Sigma^{-1}(\mathbf{p} - \mathbf{p}_k) \right) \quad (1)$$

During optimization, the covariance matrix  $\Sigma$  is factorized into a scaling matrix  $\mathbf{S}$  and a rotation matrix  $\mathbf{R}$  as  $\Sigma = \mathbf{R} \mathbf{S} \mathbf{S}^\top \mathbf{R}^\top$  to ensure its positive semidefiniteness. To obtain the rendering results of 3D Gaussians from a specific view, the 3D Gaussian is first projected to a 2D splat in screen space using the view matrix  $\mathbf{W}$  and an affine approximated

projection matrix  $\mathbf{J}$  as illustrated in [55]:

$$\Sigma' = \mathbf{J} \mathbf{W} \Sigma \mathbf{W}^\top \mathbf{J}^\top \quad (2)$$

By removing the third row and column of  $\Sigma'$ , we obtain a  $2 \times 2$  matrix, which represents the covariance matrix  $\Sigma^{2D}$  of the 2D splat  $\mathcal{G}^{2D}$ . Finally, the color of each pixel  $\mathbf{x}$  can be computed using volumetric alpha blending as follows:

$$\mathbf{c}(\mathbf{x}) = \sum_{k=1}^K \mathbf{c}_k \alpha_k \mathcal{G}_k^{2D}(\mathbf{x}) \prod_{j=1}^{k-1} (1 - \alpha_j \mathcal{G}_j^{2D}(\mathbf{x})) \quad (3)$$

where  $k$  is the index of the Gaussian primitives covering the current pixel,  $\alpha_k$  denotes the alpha values, and  $\mathbf{c}_k$  represents the view-dependent appearance modeled using Spherical Harmonics. All attributes of the 3D Gaussian primitives ( $\mathbf{p}, \mathbf{S}, \mathbf{R}, \alpha, \mathbf{c}$ ) are optimized using the photometric loss between the rendered images and the ground-truth images.

### 3.2. Nyquist-Shannon Sampling Theorem

Many signals initially exist in analog form. Sampling converts these continuous signals into a discrete format suitable for processing, storage, and transmission by digital devices. However, improper sampling can cause distortion known as aliasing. The **Nyquist-Shannon sampling theorem** states that *the sampling rate  $\nu$  must be at least twice the bandwidth of the signal to avoid aliasing*. Based on this theorem, there are two common approaches to address aliasing: one is to increase the sampling rate, which inevitably raises the computational workload; the other is to apply bandpass filters to the signals to eliminate frequencies higher than  $\nu/2$ . The frequency  $\nu/2$  is known as the Nyquist frequency.

The rendering process of 3D Gaussian Splatting involves sampling. It uses discrete pixels to sample 3D Gaussians, ultimately producing a 2D rendering result from this 3D representation. Consequently, the rendering of 3D Gaussian Splatting also faces the challenge of aliasing. Corresponding to the two approaches mentioned earlier, the first method to address aliasing in 3DGS rendering is Super Sampling [38]. This technique renders images at a higher resolution—effectively increasing the sampling rate—and then pools the high-resolution results to generate anti-aliased low-resolution images. However, the high resolution used in Super Sampling leads to additional computational burden, resulting in slower rendering speeds. The second approach applies filtering to 3D Gaussians before rendering, ensuring their frequency remains below the Nyquist limit. We adopt this method for efficient rendering. However, excessive filtering can cause signal loss, leading to overly smooth results that lack fine details. In Section 4, we will explain in detail how our method selects the appropriate filter for each Gaussian primitive.

## 4. Method

In this part, we first introduce our Level-of-Detail-Sensitive 3D Filter in Section 4.1, which takes the sampling rate as input and predicts the filters for 3D Gaussians. This design helps 3DGS disentangle the inputs of different sampling rates to better learn a pre-filtered radiance field from per-filtered images without ambiguity. Then we illustrate the EWA filter technique in Section 4.2, which is employed to enhance the anti-aliasing capabilities of our method. The overview of our method is illustrated in Figure 3.

### 4.1. Level-of-Detail-Sensitive 3D Filter

Applying zoom-in and zoom-out operations on scenes reconstructed by 3DGS can lead to noticeable visual artifacts, including erosion and dilation [50]. To solve these artifacts, Mip-Splatting proposes 3D Smoothing Filter as follows :

$$\mathcal{G}_k(\mathbf{x}) = \sqrt{\frac{|\Sigma_k|}{|\Sigma_k + \frac{s}{\nu_k}|}} e^{-\frac{1}{2}(\mathbf{x} - \mathbf{p}_k)^T (\Sigma_k + \frac{s}{\nu_k})(\mathbf{x} - \mathbf{p}_k)} \quad (4)$$

where the hyper parameter  $s$  is used to control the filter size and  $\nu_k$  is the maximal sampling rate for the  $k$ -th primitive which could be computed as follows:

$$\hat{\nu}_k = \max_{n \in \{1, \dots, N\}} \frac{f_n}{d_n} \quad (5)$$

where  $N$  is the number of training views,  $f_n$  is the focal length of the  $n$ -th view, and  $d_n$  is the distance from the  $n$ -th view to the current primitive. The time complexity of Equation 5 is  $\mathcal{O}(KN)$ , where  $K$  is the number of Gaussian primitives and  $N$  is the number of training views. To reduce computational load, Mip-Splatting recomputes  $\nu_k$  every 100 iterations. After training, the  $\hat{\nu}$  for each primitive is fixed, meaning that during testing, the filter size remains unchanged regardless of variations in the sampling rate. As a result, the training process becomes dependent on the choice of the hyperparameter  $s$ . As shown in Figure 1, Figure 2 and Figure 5, a fixed 3D smoothing filter can lead to some textures being over-filtered while others are not sufficiently filtered when the test camera moves closer or farther.

In the *Level of Detail (LOD) concept* [8, 15, 24, 40], an object’s texture resolution adapts based on the sampling rate. Inspired by this idea, we design a learnable framework that takes the sampling rates of Gaussian primitives as input and outputs appropriate 3D filters. In other words, the filter size of each primitive dynamically adjusts according to the sampling rate. To minimize the increase in computational workload of training and inference, we design a learnable Gaussian Mixture Model (GMM) module instead of using a MLP for each primitive to predict the suitable filter size and appearance change. The added GMM module can be

	PSNR $\uparrow$					SSIM $\uparrow$					LPIPS $\downarrow$				
	Full Res.	$1/2$ Res.	$1/4$ Res.	$1/8$ Res.	Avg.	Full Res.	$1/2$ Res.	$1/4$ Res.	$1/8$ Res.	Avg.	Full Res.	$1/2$ Res.	$1/4$ Res.	$1/8$ Res.	Avg.
NeRF [27]	29.90	32.13	33.40	29.47	31.23	0.938	0.959	0.973	0.962	0.958	0.074	0.040	0.024	0.039	0.044
MipNeRF [2]	32.63	34.34	35.47	35.60	34.51	0.958	0.970	0.979	0.983	0.973	0.047	0.026	0.017	0.012	0.026
Tri-MipRF [12]	32.65	34.24	35.02	35.53	34.36	0.958	0.971	0.980	0.987	0.974	0.047	0.027	0.018	0.012	0.026
3DGS [14]	28.79	30.66	31.64	27.98	29.77	0.943	0.962	0.972	0.960	0.960	0.065	0.038	0.025	0.031	0.040
Mipmap-GS [19]	28.79	30.67	31.66	28.00	29.78	0.943	0.962	0.973	0.961	0.960	0.065	0.038	0.025	0.031	0.040
Multiscale-3DGS [45]	33.36	27.15	21.41	17.61	24.88	0.969	0.951	0.875	0.764	0.890	0.031	0.032	0.067	0.126	0.064
Mip-Splatting [50]	32.81	34.49	35.45	35.50	34.56	0.967	0.977	0.983	0.988	0.979	0.035	0.019	0.013	0.010	0.019
Analytic-Splatting [21]	33.22	34.92	35.98	36.00	35.03	0.967	0.977	0.984	0.989	0.979	0.033	0.019	0.012	0.010	0.018
LOD-GS (ours)	32.90	34.88	36.43	37.27	35.37	0.966	0.977	0.984	0.990	0.979	0.036	0.019	0.012	0.008	0.019
w/o LOD filter	31.88	34.09	35.86	35.73	34.39	0.961	0.975	0.984	0.989	0.977	0.042	0.021	0.013	0.010	0.022
w/o EWA filter	32.63	34.39	35.66	35.76	34.61	0.966	0.977	0.983	0.987	0.978	0.038	0.020	0.013	0.010	0.020

Table 1. **Multi-scale Training and Multi-scale Testing on the Blender dataset [27].** Our approach demonstrates state-of-the-art performance across most metrics and is highly competitive with existing GS-based methods specifically designed for anti-aliasing, such as Multiscale-3DGS [45], Mip-Splatting [50], Mipmap-GS [18], and Analytic-Splatting [21].

expressed using the following equation:

$$\mathcal{F}(x) = \sum_{i=1}^l w_i \exp\left(-\frac{(x - \mu_i)^2}{2\sigma_i^2}\right) \quad (6)$$

where  $l$  is the number of basis functions,  $\mu_i$  and  $\sigma_i$  are the distribution center and standard deviation which will be optimized using gradient descent. The input of the GMM module is the sampling rate, defined as:  $\nu = 1/T = f/d$ , where  $f$  is the focal length and  $d$  is the distance from camera to the primitive.  $T$  is defined as the sampling interval. We also add a learnable residual in opacity to model the opacity change during the filtering, this design helps us avoid the use of hyperparameter in Equation 4. Above all, our proposed LOD sensitive filter could be represented as:

$$\mathcal{G}_k(x) = (\alpha_k + \mathcal{F}_\alpha(\nu)) e^{-\frac{1}{2}(x - \mathbf{p}_k)^T (\Sigma_k + \mathcal{F}_s(\nu))(x - \mathbf{p}_k)} \quad (7)$$

where  $\nu$  is the sampling rate of the Gaussian primitive. The sampling rate from one camera to all the primitives can be computed efficiently in  $\mathcal{O}(K)$ . This allows us to perform this computation in each iteration, rather than updating the sampling rate every 100 iterations, as done in Mip-Splatting [50]. This design makes each Gaussian primitive sensitive to changes in the sampling rate. As a result, the scale and opacity of the primitive can be adjusted accordingly. The following experimental results demonstrate that our proposed method can better bake images from different sampling rates into a single radiance field, generating aliasing-free rendering results while preserving details.

## 4.2. EWA Filtering

In the original implementation of 3DGS, a dilation operator [50] is applied to each 2D splat. This helps avoid small primitives that are hard to optimize. The dilation operator could be written as:  $\mathcal{G}_k^{2D}(x) = e^{-\frac{1}{2}(x - \mathbf{p}_k)^T (\Sigma_k^{2D} + s\mathbf{I})(x - \mathbf{p}_k)}$ . This operator leads to obvious dilation artifacts when the image resolution decreases. These artifacts are primarily

caused by the expansion of the primitive's scale without adjusting its opacity. As a result, the overall energy increases, leading to the dilation effect. Mip-Splatting [50] utilizes EWA Filtering [55] to alleviate this artifact:

$$\mathcal{G}_k^{2D}(x) = \sqrt{\frac{|\Sigma_k^{2D}|}{|\Sigma_k^{2D} + s\mathbf{I}|}} e^{-\frac{1}{2}(x - \mathbf{p}_k)^T (\Sigma_k^{2D} + s\mathbf{I})(x - \mathbf{p}_k)} \quad (8)$$

The main difference between dilation operator and EWA filter is the normalization term preceding the exponential term. In LOD-GS, we also use the EWA filter before the alpha blending computation to reduce the aliasing artifact. After the EWA filtering, we perform alpha blending to obtain the rendering result as follows:

$$\mathbf{c}(\mathbf{x}) = \sum_{k=1}^K (\mathbf{c}_k + \mathcal{F}_c(\nu)) \hat{\alpha}_k \prod_{j=1}^{k-1} (1 - \hat{\alpha}_j) \quad (9)$$

$$\hat{\alpha}_k = \sqrt{\frac{|\Sigma_k^{2D}|}{|\Sigma_k^{2D} + s\mathbf{I}|}} (\alpha_k + \mathcal{F}_\alpha(\nu)) \quad (10)$$

where  $\hat{\alpha}$  is the opacity of the filtered Gaussian primitive, and  $\mathcal{F}_c$  is a learnable module that models the slight color differences caused by changes in the sampling rate. After obtaining the rendering results, we compute the image loss between these results and the ground truth. Then we perform gradient descent to optimize all Gaussian parameters and the filter prediction module in an end-to-end manner.

## 5. Experimental Evaluation

### 5.1. Implementation

The implementation of LOD-GS follows the framework of vanilla 3DGS, which is implemented using PyTorch and CUDA code. We developed a customized CUDA rasterizer to support the forward and backward of our LOD-GS. The primitive level appearance change is fitted using a group of

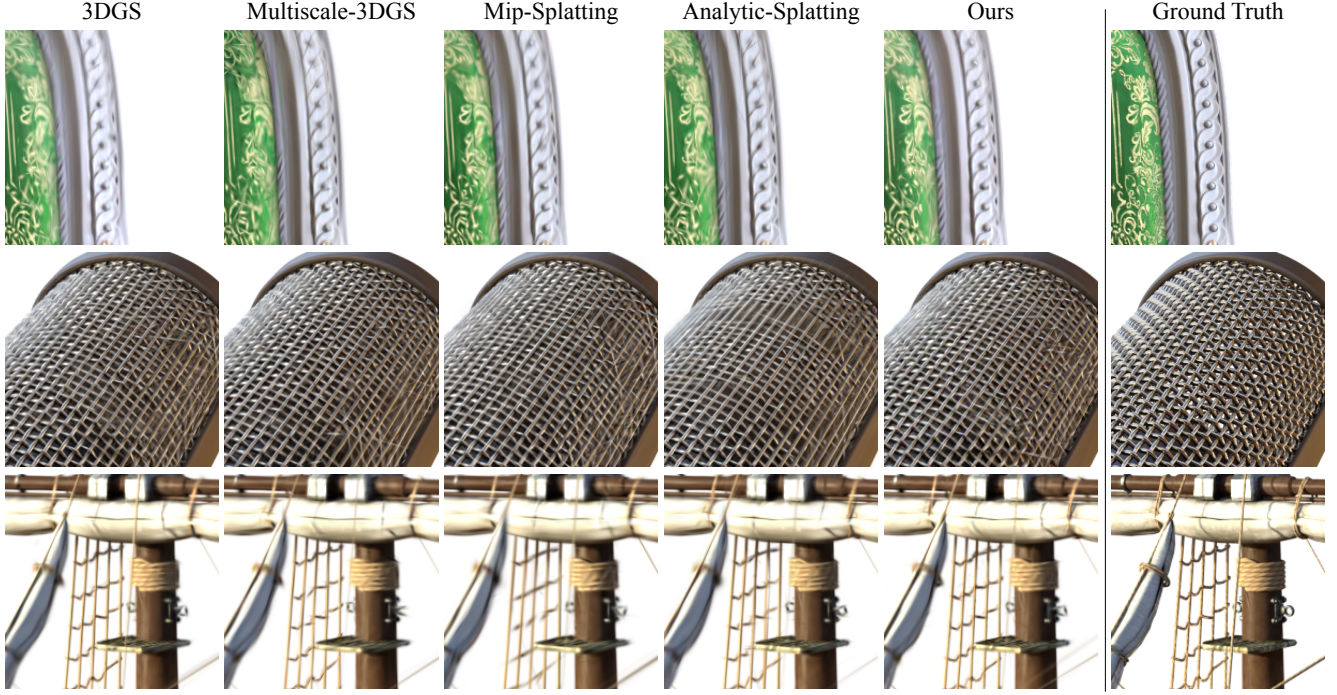


Figure 4. **Qualitative comparison on our extended Blender dataset.** All methods are trained at three levels (near, middle, and far) and tested at the near level. Our method more effectively captures the details of microstructures and textures.

	PSNR $\uparrow$				SSIM $\uparrow$				LPIPS $\downarrow$			
	Level 1	Level 2	Level 3	Avg.	Level 1	Level 2	Level 3	Avg.	Level 1	Level 2	Level 3	Avg.
3DGS [14]	27.20	32.57	37.12	32.30	0.906	0.970	0.995	0.957	0.150	0.031	0.005	0.062
Mipmap-GS [19]	26.59	31.61	34.66	30.95	0.898	0.967	0.992	0.952	0.157	0.034	0.005	0.066
Multiscale-3DGS[45]	26.31	31.54	34.66	30.84	0.898	0.967	0.992	0.952	0.158	0.034	0.005	0.066
Mip-Splatting [50]	26.87	33.08	40.76	33.57	0.902	0.973	0.997	0.957	0.154	0.029	0.003	0.062
Analytic-Splatting [21]	27.06	33.27	40.41	33.58	0.901	0.972	0.997	0.957	0.154	0.030	0.003	0.062
LOD-GS (ours)	27.30	33.40	41.27	33.99	0.905	0.973	0.997	0.958	0.148	0.030	0.003	0.060

Table 2. **Multi-level Training and Multi-level Testing on our extended Blender dataset.** Our LOD-GS achieves state-of-the-art performance in multi-level scene representation compared to vanilla 3DGS and existing anti-aliasing Gaussian splatting methods.

Gaussian functions, we set the number of these Gaussians to 20 in the synthetic dataset, and set it to 8 in Mip-NeRF 360 dataset for a smaller model size so that our machine can perform training. We evaluate our method on public datasets, including the Multi-scale Synthetic Dataset from Mip-NeRF [2] and the Mip-NeRF 360 [3] dataset. This allows us to test our performance on both synthetic scenes and real-world scenes. We also render a multi-level synthetic dataset for evaluation as illustrated in Section 5.3. All experiments are conducted on a single RTX3090 GPU.

## 5.2. Evaluation on the Multi-scale Blender Dataset

The Blender dataset introduced in the original NeRF [27] is a synthetic dataset where all training and testing images observe the scene content from a roughly constant distance with the same focal length, which differs significantly from real-world captures. MipNeRF [1] introduces a

multi-scale Blender dataset designed to enhance the evaluation of reconstruction accuracy and anti-aliasing in multi-resolution scenes. This dataset is generated by downscaling the original dataset by factors of 2, 4, and 8, and then combining these variations. We evaluate our LOD-GS on this dataset with several competitive methods, including NeRF-based methods (NeRF [27], MipNeRF [1], and Tri-MipRF [12]) and 3DGS-based methods (Mipmap-GS [18], Multiscale-3DGS [45], Mip-Splatting [50], and Analytic-Splatting [21]). Following previous works, we report three metrics: PSNR, SSIM [39], and VGG LPIPS [52] across four resolutions and average results, as shown in Table 1. Mip-NeRF and Tri-MipRF exhibit stronger anti-aliasing capabilities compared to vanilla NeRF. For 3DGS-based methods, Mip-Splatting and Analytic-Splatting significantly enhance the anti-aliasing ability of 3DGS. While Multiscale-3DGS can achieve better performance at the

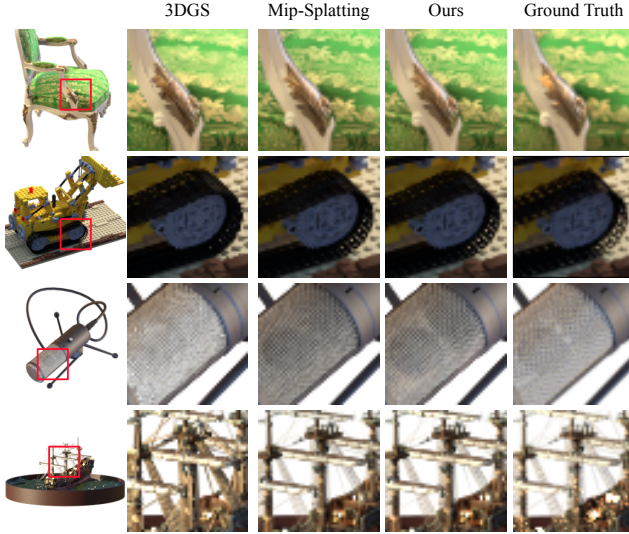


**Figure 5. Qualitative comparison on Anti-aliasing.** We compare the results of our method with the aliased rendering results of 3DGS and the anti-aliased results of Mip-Splatting to illustrate the anti-aliasing capabilities of our proposed method. The positions of the details on the original objects are marked with red boxes.

original resolution, it degenerates at lower resolutions. It is important to emphasize that both Mip-Splatting and Analytic-Splatting require sampling more cases from higher resolutions to achieve good performance. In contrast, by utilizing LOD-sensitive filter control, our method achieves rather good performance without relying on any dataset sampling technique. As shown in Table 1, our LOD-GS achieves state-of-the-art anti-aliasing performance while maintaining competitive rendering quality at the original resolution. To test the effectiveness of the modules in LOD-GS, we also performed an ablation study. The experimental results are summarized in the last two rows of the Table 1. As shown, removing either the EWA filter or the LOD filter leads to a performance drop, especially at lower resolutions. This indicate that both these two modules are crucial for the anti-aliasing of 3DGS.

### 5.3. Evaluation on the Multi-level Blender Dataset

Both decreasing the focal length and increasing the camera distance can change the sampling rate, thereby reducing the resolution of the photographed object. Mip-NeRF reduces image resolution using image processing techniques, attributing this change to alterations in focal length. However, in 3D applications, the most common approach to change the sampling rate is by adjusting the camera distance, rather than the focal length. There is a difference between adjusting the camera distance and the focal length. To make a more comprehensive evaluation, we re-render the synthetic dataset used in NeRF [27] from three different camera distances. We call this extended dataset the “Multi-

level Blender Dataset” and assign Level 1 to the camera with the nearest camera distance to the object, Level 2 to the middle camera distance, and Level 3 to the farthest distance. The results of the comparative experiments on this dataset are presented in Table 2.

**Qualitative results.** We further conducted a qualitative comparison of our LOD-GS with vanilla 3DGS and existing GS-based methods for the reconstruction of details. As shown in Figure 4, both 3DGS and Multiscale-3DGS fail to capture very fine details, resulting in noticeable discrepancies in appearance compared to the ground-truth images. Although Mip-Splatting and Analytic-Splatting retain some texture detail, they still lose additional intricacies and produce overly blurred rendering results in certain areas. In contrast, our method captures more details and achieves higher rendering quality. To be more precise, as illustrated in Figure 4, our method excels at reconstructing the small bump on the back of the chair, the intricate texture on the surface of the microphone, and the rope net of the ship. In contrast, other methods either fail to capture these fine details or produce overly blurred results.

In addition to capturing fine details, we also evaluate the anti-aliasing capabilities of our method. We render the object from a considerable distance to assess this ability. The qualitative results are illustrated in Figure 5. As shown, 3DGS tends to generate dilated boundaries and aliased results in areas with high-frequency texture. In contrast, both Mip-Splatting and our LOD-GS effectively handle aliasing when the camera is far from the scene, i.e., at a low sampling rate. Compared to Mip-Splatting, our method can reconstruct more details, such as the inner structure of the microphone, as shown in the third row of Figure 5.

### 5.4. Evaluation on the Mip-NeRF 360 Dataset

To test the performance of our method on real-world data, we evaluate our method and perform comparisons on the Mip-NeRF 360 Dataset [3]. Due to our limited computational resources, we cannot perform training on all resolutions in the dataset. Therefore, we preprocess the full-resolution images into three downsampled scales ( $1/8$ ,  $1/16$ , and  $1/32$ ) and conduct multi-scale training and testing. The qualitative and quantitative experimental results are shown in Figure 6 and Table 3, respectively. As shown in Table 3, our method achieves SOTA performance across nearly all metrics at different resolutions.

**Qualitative Results** To provide a more intuitive comparison on real-world datasets, we analyze the rendering results from different resolutions and methods. As shown in Figure 6, the  $1/8$  garden images reveal that both 3DGS and Multiscale-3DGS exhibit a blurred appearance, lacking fine details. While Mip-Splatting captures some details, its rendering results are overly smooth. Analytic-Splatting effec-

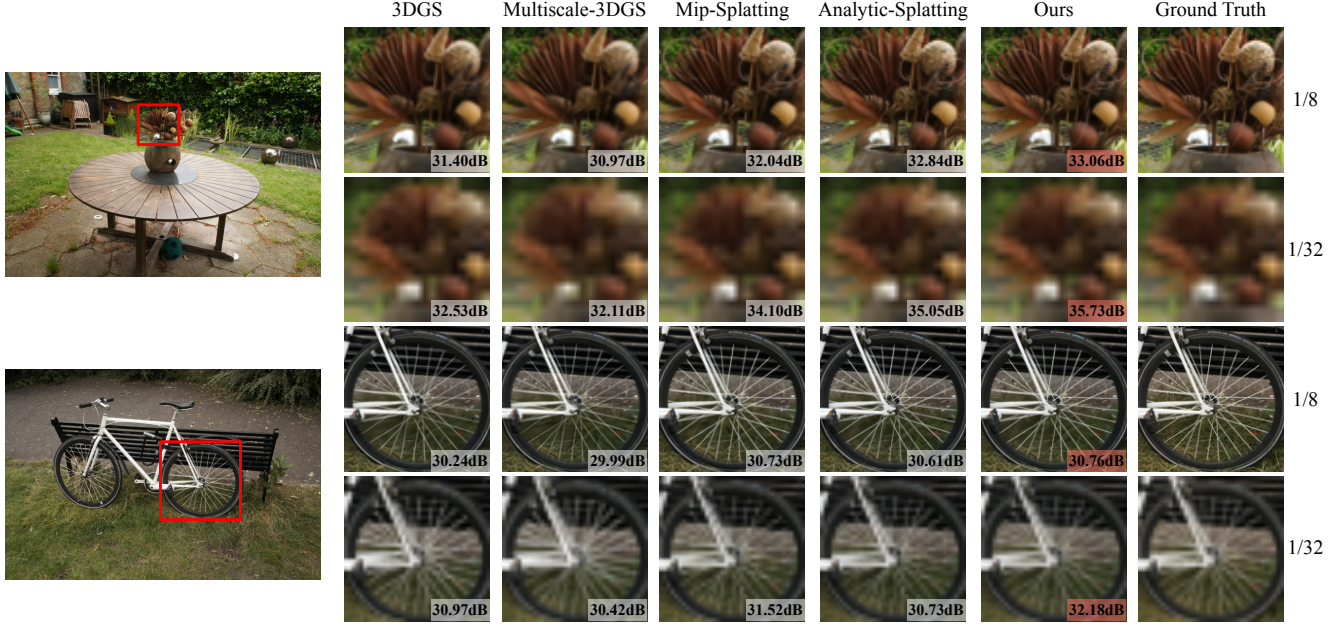


Figure 6. **Qualitative comparison on the Mip-NeRF 360 dataset [3].** All methods are trained and tested at three downsampled resolutions ( $1/8$ ,  $1/16$ , and  $1/32$ ). We select two scenes (*garden* and *bicycle*) to compare the high and low-resolution rendering results.

	PSNR $\uparrow$				SSIM $\uparrow$				LPIPS $\downarrow$			
	$1/8$ Res.	$1/16$ Res.	$1/32$ Res.	Avg.	$1/8$ Res.	$1/16$ Res.	$1/32$ Res.	Avg.	$1/8$ Res.	$1/16$ Res.	$1/32$ Res.	Avg.
3DGS [14]	27.99	29.96	29.62	29.19	0.850	0.919	0.934	0.901	0.158	0.074	0.057	0.096
Mipmap-GS [18]	27.28	29.23	28.50	28.33	0.836	0.909	0.919	0.888	0.173	0.084	0.066	0.108
Multiscale-3DGS[45]	27.30	29.25	28.50	28.35	0.836	0.910	0.920	0.888	0.173	0.084	0.066	0.108
Mip-Splatting [50]	28.35	30.16	31.06	29.86	0.865	0.924	0.949	0.913	0.132	0.064	0.043	0.080
Analytic-Splatting [21]	28.84	30.63	31.63	30.37	0.868	0.926	0.953	0.915	0.128	0.066	0.043	0.079
LOD-GS (ours)	28.96	30.90	32.40	30.75	0.869	0.929	0.958	0.919	0.134	0.065	0.038	0.079

Table 3. **Multi-scale training and Multi-scale testing on the Mip-NeRF 360 dataset [3].** All methods are trained and tested at three downsampled resolutions ( $1/8$ ,  $1/16$ , and  $1/32$ ). Our model achieves state-of-the-art performance across most metrics in comparison.

tively learns the detailed textures of objects, but our method achieves higher rendering quality than Analytic-Splatting. It is important to note that the additional workload introduced by Analytic-Splatting limits its rendering speed to around 30 FPS, whereas our method performs efficiently at approximately 45 FPS. In addition to its ability to reconstruct fine details, our LOD-GS also possesses strong anti-aliasing capabilities. Examining the rendering results of bicycle spokes at the  $1/32$  downsampled resolution, we see that 3DGS generates aliased results. MSGS reduces aliasing to some degree but introduces dilation artifacts. Mip-Splatting and Analytic-Splatting manage to remove aliasing but sacrifice the geometric details of the bicycle spokes. In contrast, LOD-GS generates better anti-aliased results while maximizing the preservation of the original image structure. Based on both quantitative and qualitative comparisons, our proposed LOD-GS achieves detail-preserved and aliasing-free rendering at the same time.

## 6. Conclusion

In this paper, we propose a Level-of-Detail-Sensitive Gaussian Splatting method, LOD-GS, to sense and learn the appearance changes caused by variations in the camera sampling rate. Compared to existing methods, our approach achieves state-of-the-art performance on anti-aliasing tasks while preserving fine details. It alleviates the ambiguity in multi-scale training by disentangling inputs with different sampling rates. To perform a comprehensive evaluation, we re-render the Synthetic NeRF dataset from different camera distances to account for sampling rate changes caused by camera distance. Experimental results demonstrate that LOD-GS can utilize multi-scale 2D images to train a pre-filtered radiance field, allowing the model to display detailed textures without aliasing across different sampling rates. LOD-GS is expected to further improve the reconstruction quality of neural radiance fields, especially when the collected images are captured at varying sampling rates.

## References

- [1] Jonathan T Barron, Ben Mildenhall, Matthew Tancik, Peter Hedman, Ricardo Martin-Brualla, and Pratul P Srinivasan. Mip-nerf: A multiscale representation for anti-aliasing neural radiance fields. In *ICCV*, 2021. 6
- [2] Jonathan T. Barron, Ben Mildenhall, Matthew Tancik, Peter Hedman, Ricardo Martin-Brualla, and Pratul P. Srinivasan. Mip-nerf: A multiscale representation for anti-aliasing neural radiance fields. In *Proceedings of the IEEE/CVF International Conference on Computer Vision (ICCV)*, pages 5855–5864, 2021. 2, 3, 5, 6
- [3] Jonathan T. Barron, Ben Mildenhall, Dor Verbin, Pratul P. Srinivasan, and Peter Hedman. Mip-nerf 360: Unbounded anti-aliased neural radiance fields. In *Proceedings of the IEEE/CVF Conference on Computer Vision and Pattern Recognition (CVPR)*, pages 5470–5479, 2022. 2, 3, 6, 7, 8
- [4] Jonathan T Barron, Ben Mildenhall, Dor Verbin, Pratul P Srinivasan, and Peter Hedman. Zip-nerf: Anti-aliased grid-based neural radiance fields. In *Proceedings of the IEEE/CVF International Conference on Computer Vision*, pages 19697–19705, 2023. 3
- [5] Robert A Brebin, Loren Carpenter, and Pat Hanrahan. Volume rendering. In *Seminal graphics: pioneering efforts that shaped the field*, pages 363–372. 1998. 1
- [6] Anpei Chen, Zexiang Xu, Andreas Geiger, Jingyi Yu, and Hao Su. Tensorf: Tensorial radiance fields. In *ECCV*, 2022. 2
- [7] Franklin C Crow. The aliasing problem in computer-generated shaded images. *Communications of the ACM*, 20(11):799–805, 1977. 1
- [8] Leila De Floriani and Enrico Puppo. Hierarchical triangulation for multiresolution surface description. *ACM Transactions On Graphics (TOG)*, 14(4):363–411, 1995. 2, 4
- [9] Stavros Diolatzis, Tobias Zirr, Alexander Kuznetsov, Georgios Kopanas, and Anton Kaplanyan. N-dimensional gaussians for fitting of high dimensional functions. In *ACM SIGGRAPH 2024 Conference Papers*, pages 1–11, 2024. 3
- [10] Sara Fridovich-Keil, Alex Yu, Matthew Tancik, Qinhong Chen, Benjamin Recht, and Angjoo Kanazawa. Plenoxels: Radiance fields without neural networks. In *CVPR*, 2022. 2
- [11] Xiang Guo, Jiadai Sun, Yuchao Dai, Guanying Chen, Xiaqing Ye, Xiao Tan, Errui Ding, Yumeng Zhang, and Jingdong Wang. Forward flow for novel view synthesis of dynamic scenes. In *Proceedings of the IEEE/CVF International Conference on Computer Vision*, pages 16022–16033, 2023. 3
- [12] Wenbo Hu, Yuling Wang, Lin Ma, Bangbang Yang, Lin Gao, Xiao Liu, and Yuewen Ma. Tri-miprf: Tri-mip representation for efficient anti-aliasing neural radiance fields. In *Proceedings of the IEEE/CVF International Conference on Computer Vision (ICCV)*, pages 19774–19783, 2023. 3, 5, 6
- [13] Yi-Hua Huang, Yang-Tian Sun, Ziyi Yang, Xiaoyang Lyu, Yan-Pei Cao, and Xiaojuan Qi. Sc-gs: Sparse-controlled gaussian splatting for editable dynamic scenes. In *Proceedings of the IEEE/CVF conference on computer vision and pattern recognition*, pages 4220–4230, 2024. 3
- [14] Bernhard Kerbl, Georgios Kopanas, Thomas Leimkühler, and George Drettakis. 3d gaussian splatting for real-time radiance field rendering. *ACM Transactions on Graphics*, 42(4), 2023. 1, 2, 3, 5, 6, 8
- [15] Eric LaMar, Bernd Hamann, and Kenneth I Joy. *Multiresolution techniques for interactive texture-based volume visualization*. IEEE, 1999. 2, 4
- [16] Christoph Lassner and Michael Zollhofer. Pulsar: Efficient sphere-based neural rendering. In *Proceedings of the IEEE/CVF Conference on Computer Vision and Pattern Recognition*, pages 1440–1449, 2021. 2
- [17] Marc Levoy. Efficient ray tracing of volume data. *ACM Transactions on Graphics (ToG)*, 9(3):245–261, 1990. 1
- [18] Jiameng Li, Yue Shi, Jiezhang Cao, Bingbing Ni, Wenjun Zhang, Kai Zhang, and Luc Van Gool. Mipmap-gs: Let gaussians deform with scale-specific mipmap for anti-aliasing rendering, 2024. 3, 5, 6, 8
- [19] Jiameng Li, Yue Shi, Jiezhang Cao, Bingbing Ni, Wenjun Zhang, Kai Zhang, and Luc Van Gool. Mipmap-gs: Let gaussians deform with scale-specific mipmap for anti-aliasing rendering. *arXiv preprint arXiv:2408.06286*, 2024. 5, 6
- [20] Zhengqi Li, Simon Niklaus, Noah Snavely, and Oliver Wang. Neural scene flow fields for space-time view synthesis of dynamic scenes. In *Proceedings of the IEEE/CVF Conference on Computer Vision and Pattern Recognition*, pages 6498–6508, 2021. 3
- [21] Zhihao Liang, Qi Zhang, Wenbo Hu, Lei Zhu, Ying Feng, and Kui Jia. Analytic-splatting: Anti-aliased 3d gaussian splatting via analytic integration. In *Computer Vision – ECCV 2024: 18th European Conference, Milan, Italy, September 29–October 4, 2024, Proceedings, Part XVII*, page 281–297, Berlin, Heidelberg, 2024. Springer-Verlag. 3, 5, 6, 8
- [22] Youtian Lin, Zuozhuo Dai, Siyu Zhu, and Yao Yao. Gaussian-flow: 4d reconstruction with dynamic 3d gaussian particle. In *Proceedings of the IEEE/CVF Conference on Computer Vision and Pattern Recognition (CVPR)*, pages 21136–21145, 2024. 3
- [23] Lingjie Liu, Jiatao Gu, Kyaw Zaw Lin, Tat-Seng Chua, and Christian Theobalt. Neural sparse voxel fields. 2020. 2
- [24] David Luebke, Benjamin Watson, Jonathan D. Cohen, Martin Reddy, and Amitabh Varshney. *Level of Detail for 3D Graphics*. Elsevier Science Inc., USA, 2002. 2, 4
- [25] Jonathon Luiten, Georgios Kopanas, Bastian Leibe, and Deva Ramanan. Dynamic 3d gaussians: Tracking by persistent dynamic view synthesis. In *2024 International Conference on 3D Vision (3DV)*, pages 800–809. IEEE, 2024. 3
- [26] Nelson Max. Optical models for direct volume rendering. *TVCG*, 1(2):99–108, 1995. 1
- [27] Ben Mildenhall, Pratul P. Srinivasan, Matthew Tancik, Jonathan T. Barron, Ravi Ramamoorthi, and Ren Ng. Nerf: Representing scenes as neural radiance fields for view synthesis. In *ECCV*, 2020. 1, 2, 5, 6, 7
- [28] Thomas Müller, Alex Evans, Christoph Schied, and Alexander Keller. Instant neural graphics primitives with a multiresolution hash encoding. *TOG*, 41(4):1–15, 2022. 2

[29] Harry Nyquist. Certain topics in telegraph transmission theory. *Transactions of the American Institute of Electrical Engineers*, 47(2):617–644, 2009. 2

[30] Keunhong Park, Utkarsh Sinha, Jonathan T Barron, Sofien Bouaziz, Dan B Goldman, Steven M Seitz, and Ricardo Martin-Brualla. Nerfies: Deformable neural radiance fields. In *Proceedings of the IEEE/CVF international conference on computer vision*, pages 5865–5874, 2021. 3

[31] Keunhong Park, Utkarsh Sinha, Peter Hedman, Jonathan T Barron, Sofien Bouaziz, Dan B Goldman, Ricardo Martin-Brualla, and Steven M Seitz. Hypernerf: a higher-dimensional representation for topologically varying neural radiance fields. *ACM Transactions on Graphics (TOG)*, 40(6):1–12, 2021. 3

[32] Sergey Prokudin, Qianli Ma, Maxime Raafat, Julien Valentin, and Siyu Tang. Dynamic point fields. In *Proceedings of the IEEE/CVF International Conference on Computer Vision*, pages 7964–7976, 2023. 2

[33] Albert Pumarola, Enric Corona, Gerard Pons-Moll, and Francesc Moreno-Noguer. D-nerf: Neural radiance fields for dynamic scenes. In *Proceedings of the IEEE/CVF conference on computer vision and pattern recognition*, pages 10318–10327, 2021. 3

[34] Claude E Shannon. Communication in the presence of noise. *Proceedings of the IRE*, 37(1):10–21, 1949. 2

[35] Cheng Sun, Min Sun, and Hwann-Tzong Chen. Direct voxel grid optimization: Super-fast convergence for radiance fields reconstruction. In *CVPR*, 2022. 2

[36] Weiwei Sun, Eduard Trulls, Yang-Che Tseng, Sneha Sambandam, Gopal Sharma, Andrea Tagliasacchi, and Kwang Moo Yi. Pointnerf++: a multi-scale, point-based neural radiance field. In *European Conference on Computer Vision*, pages 221–238. Springer, 2024. 2

[37] Edgar Tretschk, Ayush Tewari, Vladislav Golyanik, Michael Zollhöfer, Christoph Lassner, and Christian Theobalt. Non-rigid neural radiance fields: Reconstruction and novel view synthesis of a dynamic scene from monocular video. In *Proceedings of the IEEE/CVF International Conference on Computer Vision*, pages 12959–12970, 2021. 3

[38] Chen Wang, Xian Wu, Yuan-Chen Guo, Song-Hai Zhang, Yu-Wing Tai, and Shi-Min Hu. Nerf-sr: High-quality neural radiance fields using supersampling. In *Proceedings of the 30th ACM International Conference on Multimedia*, pages 6445–6454, 2022. 4

[39] Zhou Wang, Alan C Bovik, Hamid R Sheikh, and Eero P Simoncelli. Image quality assessment: from error visibility to structural similarity. *TIP*, 13(4):600–612, 2004. 6

[40] Manfred Weiler, Rüdiger Westermann, Chuck Hansen, Kurt Zimmermann, and Thomas Ertl. Level-of-detail volume rendering via 3d textures. In *Proceedings of the 2000 IEEE symposium on Volume visualization*, pages 7–13, 2000. 2, 4

[41] Lance Williams. Pyramidal parametrics. In *Proceedings of the 10th Annual Conference on Computer Graphics and Interactive Techniques*, page 1–11, New York, NY, USA, 1983. Association for Computing Machinery. 2

[42] Guanjun Wu, Taoran Yi, Jiemin Fang, Lingxi Xie, Xiaopeng Zhang, Wei Wei, Wenyu Liu, Qi Tian, and Xinggang Wang. 4d gaussian splatting for real-time dynamic scene rendering. In *Proceedings of the IEEE/CVF Conference on Computer Vision and Pattern Recognition (CVPR)*, pages 20310–20320, 2024. 3

[43] Wenqi Xian, Jia-Bin Huang, Johannes Kopf, and Changil Kim. Space-time neural irradiance fields for free-viewpoint video. In *Proceedings of the IEEE/CVF conference on computer vision and pattern recognition*, pages 9421–9431, 2021. 3

[44] Qiangeng Xu, Zexiang Xu, Julien Philip, Sai Bi, Zhixin Shu, Kalyan Sunkavalli, and Ulrich Neumann. Pointnerf: Point-based neural radiance fields. In *Proceedings of the IEEE/CVF conference on computer vision and pattern recognition*, pages 5438–5448, 2022. 2

[45] Zhiwen Yan, Weng Fei Low, Yu Chen, and Gim Hee Lee. Multi-scale 3d gaussian splatting for anti-aliased rendering. In *Proceedings of the IEEE/CVF Conference on Computer Vision and Pattern Recognition (CVPR)*, pages 20923–20931, 2024. 3, 5, 6, 8

[46] Shuojue Yang, Qian Li, Daiyun Shen, Bingchen Gong, Qi Dou, and Yueming Jin. Deform3DGS: Flexible Deformation for Fast Surgical Scene Reconstruction with Gaussian Splatting. In *proceedings of Medical Image Computing and Computer Assisted Intervention – MICCAI 2024*. Springer Nature Switzerland, 2024. 3

[47] Ziyi Yang, Xinyu Gao, Wen Zhou, Shaohui Jiao, Yuqing Zhang, and Xiaogang Jin. Deformable 3d gaussians for high-fidelity monocular dynamic scene reconstruction. In *Proceedings of the IEEE/CVF Conference on Computer Vision and Pattern Recognition (CVPR)*, pages 20331–20341, 2024. 3

[48] Zeyu Yang, Hongye Yang, Zijie Pan, and Li Zhang. Real-time photorealistic dynamic scene representation and rendering with 4d gaussian splatting. In *International Conference on Learning Representations (ICLR)*, 2024. 3

[49] Wang Yifan, Felice Serena, Shihao Wu, Cengiz Özturel, and Olga Sorkine-Hornung. Differentiable surface splatting for point-based geometry processing. *ACM Transactions On Graphics (TOG)*, 38(6):1–14, 2019. 2

[50] Zehao Yu, Anpei Chen, Binbin Huang, Torsten Sattler, and Andreas Geiger. Mip-splatting: Alias-free 3d gaussian splatting. In *Proceedings of the IEEE/CVF Conference on Computer Vision and Pattern Recognition (CVPR)*, pages 19447–19456, 2024. 3, 4, 5, 6, 8

[51] Raza Yunus, Jan Eric Lenssen, Michael Niemeyer, Yiyi Liao, Christian Rupprecht, Christian Theobalt, Gerard Pons-Moll, Jia-Bin Huang, Vladislav Golyanik, and Eddy Ilg. Recent trends in 3d reconstruction of general non-rigid scenes. In *Computer Graphics Forum*, page e15062. Wiley Online Library, 2024. 3

[52] Richard Zhang, Phillip Isola, Alexei A Efros, Eli Shechtman, and Oliver Wang. The unreasonable effectiveness of deep features as a perceptual metric. In *CVPR*, 2018. 6

[53] Yufeng Zheng, Wang Yifan, Gordon Wetzstein, Michael J Black, and Otmar Hilliges. Pointavatar: Deformable point-based head avatars from videos. In *Proceedings of the IEEE/CVF conference on computer vision and pattern recognition*, pages 21057–21067, 2023. 2

- [54] Yiyu Zhuang, Qi Zhang, Ying Feng, Hao Zhu, Yao Yao, Xiaoyu Li, Yan-Pei Cao, Ying Shan, and Xun Cao. Anti-aliased neural implicit surfaces with encoding level of detail. New York, NY, USA, 2023. Association for Computing Machinery. 3
- [55] Matthias Zwicker, Hanspeter Pfister, Jeroen Van Baar, and Markus Gross. Ewa volume splatting. In *Proceedings Visualization, 2001. VIS'01.*, pages 29–538. IEEE, 2001. 2, 4, 5